Nuclear Data for Science and Technology (1988 MITO), 645- 653, Copyright © 1988 JAERI.

INTERPLAY OF DIRECT AND COMPOUND-NUCLEUS MECHANISMS IN NEUTRON CAPTURE BY LIGHT NUCLIDES

S. Raman

Oak Ridge National Laboratory, Oak Ridge, Tennessee 37831 USA

S. Kahane

Nuclear Research Centre-Negev, Bear Sheva, Israel

J. E. Lynn

Atomic Energy Research Establishment, Harwell OX11 ORA, England

Abstract: We discuss the direct-capture theory pertaining to primary electric-dipole (E1) transitions following slow-neutron capture. For approximately 20 light nuclides that we have studied, estimates of direct-capture cross sections using optical-model potentials with physically realistic parameters are in reasonable agreement with the data. Minor disagreements that exist are consistent with extrapolations to light nuclides of generally accepted formulations of compound-nucleus capture. In dealing with nuclei "soft" to vibrations, we have considered the possible effects of coupling of the collective motion with the optical potential in the framework of R-matrix theory. In such cases, we find that the inclusion of "inelastic" channels results in systematic changes in the calculated cross sections.

Introduction

Our understanding of slow and medium energy neutron capture, and, hence, our ability to calculate neutron capture cross sections and spectra with some precision, is still very incomplete. To help redress this situation, we have been embarked for some time now on a systematic program[1-6] of exploring the applicability of direct and valence capture theory to the measurements of absolute cross sections for the primary electric-dipole transitions resulting from neutron capture. In the first stage, this program has concentrated on the light nuclides ($A<50$) and mostly on their thermal neutron capture cross sections. This paper summarizes the knowledge achieved to date.

In general it can be stated that for the range of light nuclides that we have critically examined (comprising ^{9}Be, ^{12}C, ^{13}C, ^{19}F, ^{20}Ne, ^{24,25,26}Mg, ^{32,33,34,36}S, ^{40,41,42,43,44,46}Ca, and ^{48}Ca) direct capture is indeed the predominant mechanism. In a few cases, the closely related valence-capture mechanism is also of major importance, especially when dealing with capture in strong neutron resonances. In most of the above cases, the relatively minor differences between the estimates of absolute cross sections from an optical-model formulation of the direct-capture theory and experimentally measured cross sections can be attributed plausibly to admixtures of compound-nucleus capture processes that have been well formulated in a semiempirical fashion from studies of resonance capture by heavier nuclides. The direct capture estimates and comparisons with data from the Mg, S, and Ca isotopes are given in a table below.

In a few cases, the discrepancies between theory and data do not possess the statistical behavior expected from an explanation based on a compound-nucleus admixture. For these cases we have postulated that there may be coupling between single-particle motion within the field of the target ground state and motion in the field of an excited collective state owing to the higher multipoles of the potential generated by the deformation of the target nucleus. Such couplings can give rise to additional contributions to the capture transition amplitude, and these additional terms can, in certain circumstances, be correlated, over a range of final states, with the direct-capture amplitude. We invoke this mechanism in the cases of ^{26}Mg and ^{44}Ca.

Theory of Direct Capture

In the ideal model of direct capture, the incident neutron is scattered by a smooth potential field representing the target nucleus A while the electromagnetic coupling causes the scattered neutron to fall into a bound single-particle orbit of the same potential. During this process, the core of the target nucleus remains undisturbed from its initial state. In calculating the matrix element for the electromagnetic transition, it is important to represent the initial state (scattering) wave function and the final state (single-particle) wave function as accurately as possible. It was recognized in the original formulation of the theory[7] that the major contribution to the radial integral comes from the external (channel) region of the configuration space where the neutron-nucleus separation is greater than the potential radius. Hence the computation of the projections of the wave functions in the channel region is emphasized in our work.

For the initial state, we employ a physically reasonable optical model in which the imaginary component of the potential accounts, in an average way, for the absorption out of the channel into the complicated states of the compound nucleus. The optical model must be adjusted in some manner (as discussed in more detail below) to reproduce the measured neutron

scattering length of the nuclide under consideration. The final state is an actual energy level of the (A+1) nucleus. Normally this state carries only a fraction of the single-particle content given by the spectroscopic factor measured in the (d,p) reaction. The "tail" of the single-particle wave function is the important part in contributing to the matrix element and its behavior is governed mainly by the binding energy of the final state. Hence we calculate the single-particle wave function for a potential well described by most of the parameters (radius, diffuseness, etc.) of the real part of the optical potential but with the well depth adjusted to reproduce the final-state binding energy.

To obtain the initial-state wave function that gives the correct neutron scattering length, we use two methods. We start from a global optical model (such as that of Moldauer[8]) that reproduces a wealth of neutron strength function and/or fast neutron scattering data. Usually we can then adjust one or more parameters (such as surface diffuseness or magnitude of imaginary potential) within physically reasonable limits to obtain the measured scattering length. This procedure leads to a specialized optical model [S] for a nuclide under study and the direct-capture cross section can be obtained immediately from this model. The initial and final-state wave functions, the integrand of the electric-dipole matrix element, and the corresponding cumulative integral leading to the potential-capture cross section are shown in Fig. 1 for the particular example of ^{44}Ca. The initial-state wave function is consistent with the measured thermal neutron scattering length of 1.41 fm. Also shown in Fig. 1, for comparison, is the equivalent channel-capture approximations discussed in Refs. 2, 3, 6, and 7.

Alternatively, we can stay with the global potential model [G] to estimate the potential-capture cross section. This model, however, yields a thermal neutron potential scattering length which, in general, is different from the measured value. In Fig. 1 (see the initial-state wave function given in the top panel on the right-hand side), the [G] method yields a

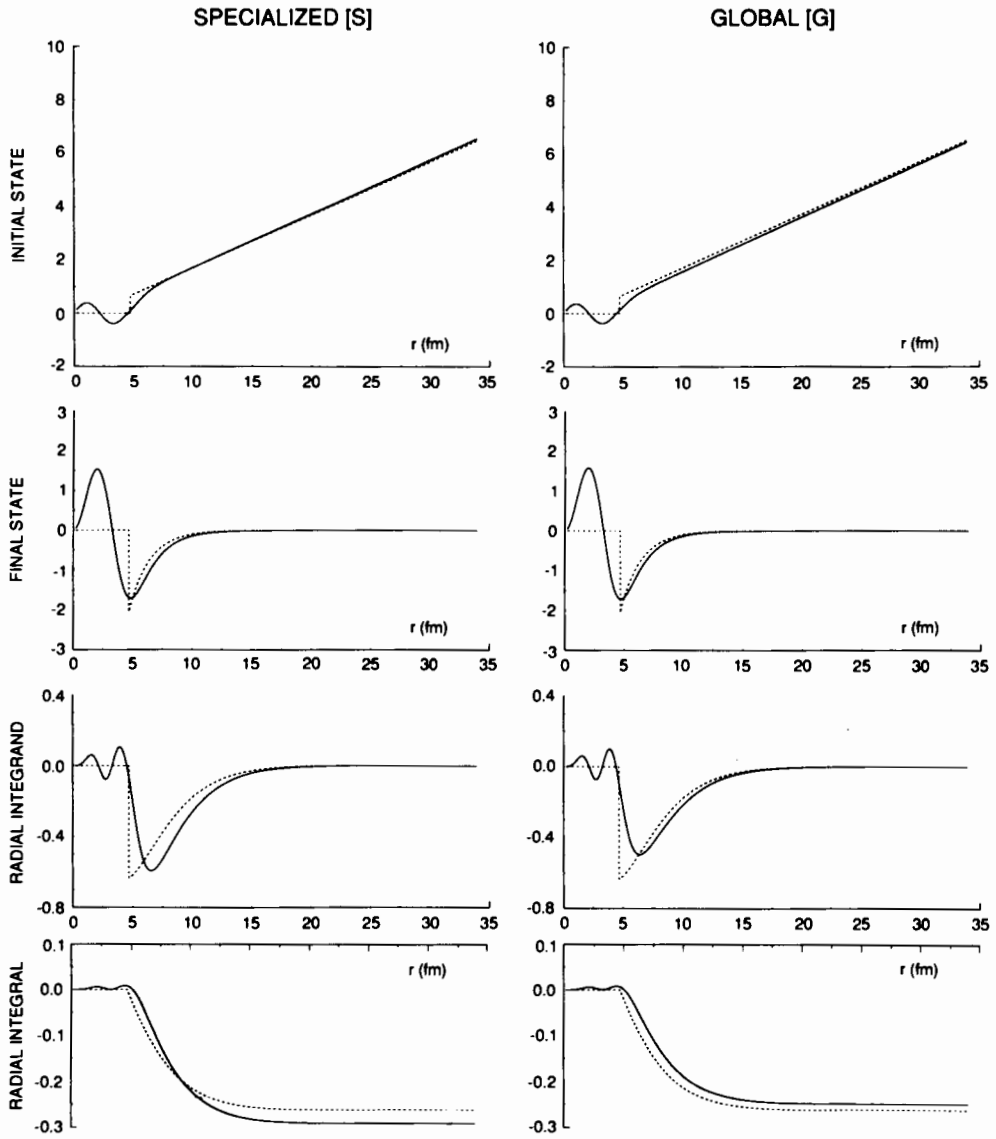

FIG. 1. Initial-state and final-state wave functions, radial integrand, and radial integral calculated for the 5.980-MeV transition in ^{45}Ca using either a specialized [S] or a global [G] optical model. The dashed lines correspond to the channel-capture approximation discussed in Ref. 2.

scattering length of 2.18 fm compared to the measured value of 1.41 fm. We account for this difference as being due to the effect of the nearby (local) resonance levels. The component of their wave functions corresponding to a projection on the elastically scattered neutron channel is directly proportional to the effect of these levels on the scattering length. The overlap of these projections with the single-particle component of the final state gives the valence-capture amplitude [V]. Its magnitude for averaged resonance levels can be estimated using the imaginary part of the initial wave functions of the global calculation. The valence-capture amplitude, while being closely related to the potential-capture amplitude, is a little more sensitive to the components of the wave function in the internal region because the initial-state wave function has an antinode rather than a node close to the potential radius. The sum (not shown in Fig. 1) of the global and valence amplitudes [G+V] results in changes to the wave function and integral of the [G] part of Fig. 1 that make them much closer to the [S] part of Fig. 1.

We have applied such a detailed analysis to a large number of electric-dipole transitions observed following thermal neutron capture by several light nuclides (see Refs. 1, 5, and 6 for the experimental data). For many of these cases, we have either improved the calculational procedure since the original publications or made changes in the experimental data on the basis of new measurements. The updated results are presented in Table 1. The global potential used is the modified Moldauer potential, the

TABLE 1. Direct capture cross sections for primary $E1$ transitions in the (n,γ) reaction on light isotopes. Columns 1, 2, and 3 give the energy, J^π value, and the (d,p) spectroscopic strength of the final state. Column 4 is the primary transition energy (essentially the binding energy of the final state). Column 5 is the average valency capture width and column 6 the potential capture cross section, both calculated using a global optical potential. The entries in column 5 do not include the spin-coupling factor and the spectroscopic factor; those in column 6 do. Column 7 is the calculated cross section using the global plus valence [G+V] procedure. Column 8 contains the calculated cross sections from the specialized optical-model procedure [S]. The experimentally determined cross sections are given in column 9. Finally, column 10 gives the minimum hypothesized compound-nucleus cross sections deduced from the differences between column 7 and column 9. In the table subheadings, a(X) refers to the experimental scattering length, while a(G) and Γ_n^o/D refer to the scattering length and the neutron strength function respectively both calculated using the global optical potential.

E_f (MeV)	J_f^π[a]	(d,p)[b] $(2J_f+1)S$	E_γ (MeV)	$(\Gamma_{\gamma,\mathrm{val}}/DE_\gamma^3)$ $\times 10^7$ (MeV^{-3})	$\sigma_{\mathrm{pot},\gamma}$ (mb)	$\sigma_{\mathrm{dir},\gamma}$[G+V] (mb)	$\sigma_{\mathrm{dir},\gamma}$[S] (mb)	σ_γ[X][c] (mb)	$\sigma_{\mathrm{CN},\gamma}$ (mb)
(A). ^{24}Mg(n,γ)^{25}Mg reaction; a(X) = 5.46 fm; a(G) = 4.50 fm; $\Gamma_n^o/D = 4.61 \times 10^{-5}$									
3.413	$3/2^-$	1.06	3.917	0.344	40.6	15.8	15.8	31.6 ± 2.2	2.7
4.276	$1/2^-$	0.40	3.054	0.402	11.4	5.2	5.2	8.3 ± 0.8	0.4
4.722	$1/2^-$	0.016	2.608	0.475	0.41	0.21	0.21	<0.03	0.1
	$3/2^-$			0.521	0.48	0.24	0.25		
5.116	$1/2^-$	0.028	2.214	0.561	0.65	0.35	0.36	0.17 ± 0.04	0.03
(B). ^{25}Mg(n,γ)^{26}Mg reaction; a(X) = 3.52 fm; a(G) = 4.41 fm; $\Gamma_n^o/D = 4.76 \times 10^{-5}$									
6.876	3^-	1.18	4.216	0.301(j=3/2)	8.0	14.5	13.8	10.9 ± 1.2	0.3
				0.266(j=1/2)	6.6	12.2	11.6		
7.261	2^-	1.48	3.832	0.332(j=3/2)	9.5	16.6	15.9	32 ± 3	3.6
				0.296(j=1/2)	7.9	14.1	13.5		
	3^-			0.332(j=3/2)	9.5	16.6	15.9		
				0.296(j=1/2)	7.9	14.1	13.5		
7.349	3^-	1.14	3.744	0.340(j=3/2)	7.2	12.5	12.0	10.7 ± 1.2	0.07
				0.304(j=1/2)	6.0	10.7	10.2		
7.542	2^-	0.36	3.551	0.360(j=3/2)	2.2	3.8	3.6	8.4 ± 0.9	1.2
				0.322(j=1/2)	1.9	3.2	3.1		
	3^-			0.360(j=3/2)	2.2	3.8	3.6		
				0.322(j=1/2)	1.9	3.2	3.1		
(C). ^{26}Mg(n,γ)^{27}Mg reaction; a(X) = 4.74 fm; a(G) = 4.31 fm; $\Gamma_n^o/D = 4.96 \times 10^{-5}$									
3.562	$3/2^-$	1.6	2.882	0.427	50.7	38.9	39.2	18.8 ± 1.3	3.6
4.828	$1/2^-$	0.63	1.615	0.711	11.1	9.2	9.3	5.3 ± 0.5	0.8
	$3/2^-$			0.769	12.3	10.2	10.3		
5.422	$3/2^-$	0.008	1.022	1.218	0.10	0.09	0.09	<0.04	0.03
5.926	$1/2^-$	0.046	0.518	2.207	0.30	0.27	0.27	0.19 ± 0.03	0.01
	$3/2^-$			2.326	0.32	0.29	0.29		

TABLE 1 (continued).

E_f (MeV)	J_f^{π}[a]	(d,p)[b] $(2J_f+1)S$	E_γ (MeV)	$(\Gamma_{\gamma,\mathrm{val}}/DE_\gamma^3) \times 10^7$ (MeV^{-3})	$\sigma_{\mathrm{pot},\gamma}$ (mb)	$\sigma_{\mathrm{dir},\gamma}$[G+V] (mb)	$\sigma_{\mathrm{dir},\gamma}$[S] (mb)	σ_γ[X][c] (mb)	$\sigma_{\mathrm{CN},\gamma}$ (mb)
				(D). ^{32}S(n,γ)^{33}S reaction; a(X) = 2.74 fm; a(G) = 3.80 fm; $\Gamma_n^o/D = 1.58 \times 10^{-4}$					
3.221	$3/2^-$	1.90	5.421	0.567	178.5	325.6	322.3	302 ± 27	0.4
4.211	$3/2^-$	0.30	4.431	0.712	24.0	41.4	41.1	25.2 ± 2.3	2.0
4.918	$1/2^-$	0.09	3.724	0.757	5.2	8.8	8.7	13.5 ± 1.3	0.5
5.711	$1/2^-$	1.06	2.931	0.994	50.8	80.4	79.7	87 ± 9	0.1
5.889	$3/2^-$	0.44	2.753	1.189	22.8	35.5	35.2	28.7 ± 2.8	0.4
6.425	$1/2^-$	0.34	2.217	1.350	12.7	19.0	18.9	13.3 ± 1.2	0.9
	$3/2^-$			1.490	14.3	21.3	21.2		
7.188	$3/2^-$	0.18	1.454	2.290	4.9	6.9	6.9	2.8 ± 0.3	0.9
				(E). ^{33}S(n,γ)^{34}S reaction; a(X) = 4.68 fm; a(G) = 3.70 fm; $\Gamma_n^o/D = 1.26 \times 10^{-4}$					
4.624	3^-	1.68	6.792	0.446(j=3/2)	23.8	10.0	9.9	24.2 ± 2.3	3.1
5.680	2^-	2.60	5.737	0.544(j=3/2)	65.2	30.1	29.9	43 ± 4	3.0
				0.460(j=1/2)	52.2	23.4	23.2		
	3^-			0.544(j=3/2)	65.2	30.1	29.9		
5.756	1^-	1.68	5.661	0.552(j=3/2)	41.7	19.4	19.3	18.4 ± 1.8	0.2
				0.468(j=1/2)	33.5	15.1	15.0		
6.169	3^-	1.00	5.248	0.603(j=3/2)	23.4	11.3	11.2	11.8 ± 1.1	0.01
6.342	1^-	0.80	5.075	0.626(j=3/2)	18.2	8.9	8.9	0.4 ± 0.1	5.6
				0.536(j=1/2)	14.9	7.1	7.1		
6.479	1^-	3.64	4.938	0.646(j=3/2)	80.9	40.0	40.0	22.2 ± 2.1	2.6
				0.554(j=1/2)	66.4	32.2	32.0		
6.685	0^-	1.28	4.731	0.678(j=3/2)	27.4	13.8	13.8	1.6 ± 0.2	6.0
	1^-			0.678(j=3/2)	27.4	13.8	13.8		
				0.584(j=1/2)	22.6	11.2	11.1		
	2^-			0.678(j=3/2)	27.4	13.8	13.8		
				0.584(j=1/2)	22.6	11.2	11.1		
	3^-			0.678(j=3/2)	27.4	13.8	13.8		
6.954	2^-	0.84	4.462	0.724(j=3/2)	17.1	8.8	8.8	7.9 ± 0.8	0.02
				0.626(j=1/2)	14.2	7.2	7.2		
7.110	$(3)^-$	0.52	4.306	0.753(j=3/2)	10.3	5.4	5.4	8.3 ± 0.8	0.3
7.630	3^-	3.92	3.787	0.868(j=3/2)	69.0	37.8	37.9	26.5 ± 2.5	1.0
7.781	1^-	1.08	3.636	0.907(j=3/2)	18.3	10.2	10.2	5.2 ± 0.6	0.8
				0.797(j=1/2)	15.6	8.6	8.6		
8.138	0^-	1.04	3.279	1.014(j=3/2)	16.0	9.2	9.2	3.2 ± 0.4	1.6
	1^-			1.014(j=3/2)	16.0	9.2	9.2		
				0.898(j=1/2)	13.8	7.8	7.8		
	2^-			1.014(j=3/2)	16.0	9.2	9.2		
				0.898(j=1/2)	13.8	7.8	7.8		
	3^-			1.014(j=3/2)	16.0	9.2	9.2		
				(F). ^{34}S(n,γ)^{35}S reaction; a(X) = 3.40 fm; a(G) = 3.59 fm; $\Gamma_n^o/D = 1.39 \times 10^{-4}$					
2.348	$3/2^-$	2.04	4.638	0.717	174.9	194.7	196.0	163 ± 15	1.4
3.802	$3/2^-$	0.36	3.184	1.083	21.6	23.6	23.8	18.2 ± 1.7	0.4
4.189	$1/2^-$	0.28	2.797	1.111	12.9	14.0	14.1	15.9 ± 1.5	0.06
4.903	$1/2^-$	1.55	2.083	1.536	53.8	58.0	58.2	46 ± 5	0.7
4.963	$3/2^-$	0.87	2.023	1.744	32.8	35.3	35.4	33.6 ± 3.0	0.02

TABLE 1 (continued).

E_f (MeV)	J_f^{π}[a]	(d,p)[b] $(2J_f+1)S$	E_γ (MeV)	$(\Gamma_{\gamma,val}/DE_\gamma^3)$ $\times 10^7$ (MeV^{-3})	$\sigma_{pot,\gamma}$ (mb)	$\sigma_{dir,\gamma}$[G+V] (mb)	$\sigma_{dir,\gamma}$[S] (mb)	σ_γ[X][c] (mb)	$\sigma_{CN,\gamma}$ (mb)
(G). ^{40}Ca(n,γ)^{41}Ca reaction; a(X) = 4.64 fm; a(G) = 2.52 fm; $\Gamma_n^o/D = 1.87 \times 10^{-4}$									
1.943	$3/2^-$	2.53	6.421	0.615	647	197	205	167 ± 25	1.2
2.462	$3/2^-$	0.90	5.901	0.690	210	66	68	31 ± 5	6.5
3.614	$1/2^-$	0.22	4.750	0.755	34	12	12	9 ± 2	0.2
3.944	$1/2^-$	1.09	4.419	0.835	155	56	58	86 ± 13	3.2
4.603	$3/2^-$	0.15	3.760	1.228	21	8	8	13 ± 3	0.6
4.753	$1/2^-$	0.35	3.611	1.094	40	16	16	30 ± 5	2.2
(H). ^{42}Ca(n,γ)^{43}Ca reaction; a(X) = 3.31 fm; a(G) = 2.25 fm; $\Gamma_n^o/D = 2.70 \times 10^{-4}$									
0.593	$3/2^-$	0.30	7.340	0.685	95	58	51	48 ± 8	0.47
2.046	$3/2^-$	2.73	5.886	0.931	673	426	387	393 ± 60	0.67
2.611	$1/2^-$	0.27	5.322	0.860	49	32	29	37 ± 6	0.18
2.878	$1/2^-$	0.19	5.055	0.928	33	21	19	18 ± 3	0.12
2.943	$3/2^-$	0.20	4.990	1.157	41	26	24	28 ± 4	0.04
3.286	$3/2^-$	0.13	4.647	1.266	24	16	15	21 ± 5	0.34
3.572	$3/2^-$	0.16	4.360	1.371	28	18	17	25 ± 4	0.57
4.207	$1/2^-$	0.85	3.726	1.406	104	70	65	65 ± 10	0.09
(I). ^{44}Ca(n,γ)^{45}Ca reaction; a(X) = 1.41 fm; a(G) = 2.18 fm; $\Gamma_n^o/D = 3.87 \times 10^{-4}$									
1.435	$3/2^-$	0.43	5.980	1.232	106	139	146	95 ± 10	4.2
1.900	$3/2^-$	2.35	5.515	1.370	524	686	723	460 ± 46	22.5
2.249	$1/2^-$	0.35	5.166	1.219	61	79	85	85 ± 10	0.1
2.842	$3/2^-$	0.40	4.573	1.736	71	92	98	35 ± 5	13.5
3.241	$3/2^-$	0.13	4.173	1.941	21	26	28	21 ± 4	0.3
3.418	$1/2^-$	0.68	3.996	1.727	88	112	122	95 ± 10	0.7
3.783	$3/2^-$	0.11	3.632	2.290	15	19	20	8 ± 3	2.3
	$1/2^-$			1.953	13	16	18		1.4
3.838	$(1/2)^-$	0.24	3.577	1.991	27	35	38	14 ± 3	4.7
4.616	$1/2^-$	0.40	2.799	2.695	34	42	47	31 ± 5	0.8
5.000	$(1/2)^-$	0.47	2.415	3.210	33	41	45	16 ± 4	5.8
(J). ^{48}Ca(n,γ)^{49}Ca reaction; a(X) = 0.38 fm; a(G) = 3.38 fm; $\Gamma_n^o/D = 6.35 \times 10^{-4}$									
0.0	$3/2^-$	3.56	5.147	2.205	401	1169	1186	818 ± 110	31.2
2.023	$1/2^-$	2.06	3.123	3.449	117	294	312	272 ± 40	0.4

parameters of which are briefly outlined in Ref. 5.

The results of the calculations for the direct capture cross sections are given in columns 7 and 8 of Table 1 and the experimental data with which they should be compared are in column 9. It can be seen there that in nearly every case there is good agreement, for individual transitions, to within a factor of about two; for some nuclides much better agreement even for a whole sequence of them. A particularly striking case of agreement is that of ^{42}Ca. When the analysis reported in Ref. 5 was done, the scattering length of this nucleus was unknown, but it was noted there that very good agreement between theory and data could be obtained if the scattering length were assumed to be a = 3.4 fm. This scattering length has now been measured[9] as a(x) = 3.31 ± 0.10 fm. Table 1 shows that direct capture is the predominant mechanism for all the nuclides listed there; this is also the case for ^{9}Be, ^{12}C, and ^{13}C (Ref. 4).

It is our hypothesis that any remaining discrepancies between theory and data are due to admixtures of statistical compound nucleus capture. We can extract an estimate of the compound nucleus cross section for each transition by use of the relation

$$\sigma_\gamma(X) = (\sigma_{dir,\gamma}^{1/2} \pm \sigma_{CN,\gamma}^{1/2})^2 . \qquad (1)$$

The $\sigma_{CN,\gamma}$ values are listed in the last column of Table 1. We can test the magnitude of this quantity by dividing $\sigma_{CN,\gamma}$ by E_γ^3 and then extracting an estimate of the compound-nucleus particle radiation width $\Gamma_{CN,\lambda\gamma}$ from

$$\frac{\Gamma_{CN,\lambda\gamma}/E_\gamma^3}{E_\lambda} \approx \frac{k(\sigma_{CN,\gamma}/E_\gamma^3)}{2\pi R R^{loc}} \qquad (2)$$

where k is the neutron wave number, R is the nuclear potential radius, E_λ is the energy of the compound-nucleus resonance responsible for thermal capture, and R^{loc} is the contribution to the R function from local levels. The reduced R function is given by Eq. (19) of Ref. 1 in terms of the reduced neutron widths. We find RR^{loc}

from $RR^{loc} = a(G)-a(X)$. The extraction of the compound-nucleus partial radiation width can be applied to individual transitions or to the average of $(\sigma_{CN,\gamma}/E_\gamma{}^3)$ for all the primary electric-dipole transitions in a given nuclide. The quantity $F = \Gamma_{CN,\gamma}/E_\gamma{}^3 E_\lambda$ can then be compared with the ratio $C = \langle\Gamma_{CN,\gamma}/E_\gamma{}^3\rangle/D$ given by the Cameron[11] semiempirical survey of total radiation widths covering a wide range of medium and heavy nuclides. He gives

$$C \approx 0.33 \times 10^{-9} A^{2/3}\ \mathrm{MeV}^{-3} . \qquad (3)$$

In general, the magnitude of $\langle F\rangle$ for a given nuclide is expected to be rather greater than the Cameron ratio because $|E_\lambda|$ will be a random fraction ($\lesssim 1$) of the mean level spacing D. Because of the Porter-Thomas distribution for partial widths, individual values of F or averages formed from a very small number of transitions can be expected to fluctuate considerably about the Cameron ratio. The deduced average values of F are shown in Table 2 alongside the Cameron ratio. We stress that Eq. (2) depends on the assumption that only one level is dominating both RR^{loc} and $\sigma_{CN,\gamma}$. Comment on the validity of this assumption is given in the final column of Table 2.

In Table 2 we notice first that there are about as many negative as positive values of F showing, as expected, that the dominant resonance in thermal-neutron compound-nucleus capture is as often bound as unbound. Secondly, we note that the values of $|\langle F\rangle|$ usually lie within an order of magnitudes of the Cameron ratio. The exceptions to this statement are ^{13}C, ^{26}Mg, ^{34}S, and ^{44}Ca. In the ^{13}C case discussed in Ref. 4, $\langle F\rangle$ is low by two orders of magnitude; however, only one transition is included in the average and ^{13}C is a light nucleus in which compound nucleus effects might be minimal. The $\langle F\rangle$ value for ^{34}S is ~20 times the C value, but the uncertainty in $\langle F\rangle$ is large and the theoretical estimates are within three standard deviations of the experimental cross sections (see Table 1). The ^{26}Mg and ^{44}Ca cases are discussed below.

TABLE 2. Summary of apparent compound nucleus contributions. The quantity $\langle F\rangle$ is obtained using Eq. (2) with $R\mathcal{R}^{loc}$ of column 2. Ratio of $\langle F\rangle/C$ is expected to be D/E_λ if compound nucleus capture and $R\mathcal{R}^{loc}$ are both dominated by a single level at E_λ. The energy $E_{\lambda(un)}$ of the first strong *unbound* level and its contribution $R\mathcal{R}^{un}$ to $R\mathcal{R}^{loc}$ are given in columns 3 and 4 respectively. These quantities give some additional information on the validity of the single-level assumption, on which comment is made in the final column. Resonance parameters leading to $R\mathcal{R}^{un}$ are from Ref. 10, except for ^{48}Ca (C. H. Johnson, priv. comm.).

Nucleus	$R\mathcal{R}^{loc}$ (fm)	$E_{\lambda(un)}$ (KeV)	$R\mathcal{R}^{un}$ (fm)	$\langle F\rangle^b$	C^b	Comments
^{24}Mg	−0.96	656	~0.01	−10	2.7	Strong evidence for single weakly bound level.
^{25}Mg	0.89	20	1.1	15	2.8	20 keV resonance at ~1/5 level spacing probably most significant contributor to CN capture.
^{26}Mg	−0.43	300?[a]	1.2	−140	2.9	Evidence for single weakly bound level, probably with $R\mathcal{R}_\lambda \approx -1.5$, reducing $\langle F\rangle$ to ~−40.
^{32}S	1.06	103	1.08	33	3.3	103 keV resonance at ~1/3 level spacing probably most significant contributor to CN capture.
^{33}S	−0.98	202	0.03	−11	3.4	Evidence for single weakly bound level with $R\mathcal{R}_\lambda \approx R\mathcal{R}^{loc}$.
^{34}S	0.19	301	0.07	64	3.5	$\langle F\rangle$ has large uncertainty.
^{40}Ca	−2.12	132	0.17	−5.8	3.8	Evidence for single weakly bound level with $R\mathcal{R}_\lambda \approx R\mathcal{R}^{loc}$.
^{42}Ca	−1.06	37	0.33	−1.3	4.0	Picture suggests strong and relatively strongly bound level(s).
^{44}Ca	0.77	52	0.8	61	4.1	52 keV level at ~2.5 level spacing probably most significant contributor to CN capture; emphasizes discrepancy between $\langle F\rangle$ and C.
^{48}Ca	3.00	450	0.1	22	4.4	Evidence for single weakly bound level.

[a] Quoted as a *p*-wave resonance in Ref. 10, but its large width makes an *s*-wave assignment possible.
[b] In units of $(10^{-9}\ \mathrm{MeV}^{-3})$.

Modification of direct capture by collective motion

We notice that for a few of the nuclides in Table 1, the discrepancies between the theoretical estimates of the direct-capture cross section and the measured capture cross sections are not only considerably greater than would be expected from the Cameron estimate of the compound nucleus contribution from a typical resonance level, but also appear as if they might be systematic in nature. A case in point is ^{26}Mg, but the most disturbing example is ^{44}Ca, for which the systematic deviation between experiment and theory is particularly strong.

These are mid-shell nuclides. Their spectra display collective features; in particular, ^{26}Mg and ^{44}Ca have the spectral charac-

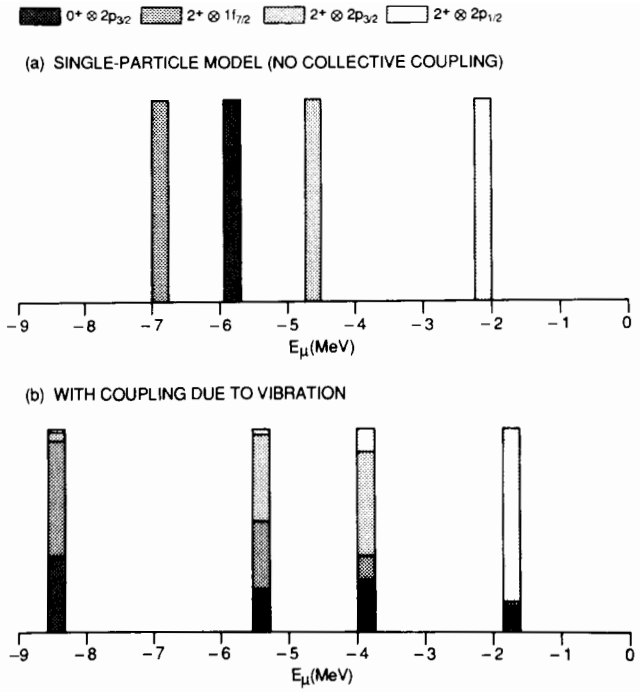

FIG. 2. Final $J^{\pi} = 3/2^{-}$ states in ^{45}Ca.

teristics of spherical nuclei soft to quadrupole vibrations. The potential field that such nuclei present to an incoming neutron is not rigidly spherical but contains terms with higher spherical harmonics that are proportional to the instantaneous deformation parameters of the nucleus. These higher multipole terms couple the initial scattering configuration (target ground state ⊗ single particle motion within spherical potential) to other configurations (target excited collective state ⊗ single particle motion). For slow-neutron scattering the resulting excitation of other configurations is virtual but the neutron scattering length is modified.

The higher multipole terms have a similar mixing effect on the final states. What would, in the absence of other residual terms in the Hamiltonian, be a state described as (target ground ⊗ single particle state b) becomes mixed with its neighbors of character (collective ⊗ single particle state b′). The latter components would not be accessible in direct capture by a rigid spherical nucleus. They would however be accessible to transitions from the virtual excitations of collective states involved in scattering by a deformable nucleus.

Thus, the capture process by such a nucleus involves the following elements. The modification of the scattering length will, to first order, not in itself involve a significant change in the calculated direct capture cross-section; a specialized optical-model calculation that reproduces the modified scattering length will give the basic term in the capture cross-section. Similarly, the modification of the final state will not, in itself, affect the deduced capture; the content of (ground state ⊗ single particle) configuration is given by the (d,p) spectroscopic factor. On the other hand, the degree of virtual excitation to (collective state 1 ⊗ single-particle state b′) will give rise to a component in the capture amplitude for the transition to the component (collective state 1 ⊗ single particle state b) in the final state. This mechanism will change the value of the potential capture cross section from the value found by the normal procedure for a rigidly spherical nucleus. To the extent that the actual final state are fragmentations of a given final state of the collectively-coupled Hamiltonian without other kinds of residual terms, the deviations between the direct capture calculated for the collective model and that for the rigid model should be systematic.

The detailed application of this concept to the case of capture by ^{44}Ca is illustrated with the help Figs. 2, 3, and 4. Fig. 2(a) shows the (^{44}Ca core ⊗ odd-parity single-particle) state spectrum for $J^{\pi} = 3/2^{-}$ states of a rigidly spherical nucleus. Single-particle energies are guided by the known picture of spectroscopic strengths near ^{44}Ca. The excitation energy of the vibrational 2^{+} state is 1.16 MeV for ^{44}Ca. On introducing the quadrupole coupling appropriate for ^{44}Ca, the spectrum shown in Fig. 2(b) is obtained. We note that 61% of the $0^{+} \otimes 2p_{3/2}$ configuration is contained in the lowest two states.

The effect of the quadrupole coupling on the potential scattering and capture can be illustrated by discussing the R-matrix expansions for the initial-state scattering. We first consider the R-matrix description of s-wave ($J^{\pi} = 1/2^{+}$) scattering by a real potential well (with our global optical-model parameters for ^{44}Ca). For the rigid spherical target and a

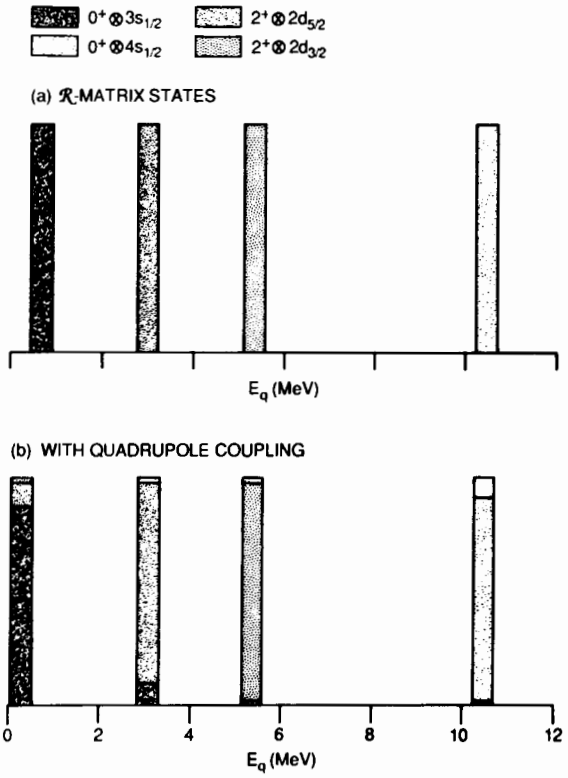

FIG. 3. R-matrix states for the construction of the $1/2^{+}$ initial scattering state of ^{44}Ca. Only the central portion of the spectrum is shown. The boundary condition for the $s_{1/2}$ single-particle R-matrix states is zero. That for the d-states is for effective asymptotic neutron energy of -1.16 MeV (i.e., minus the one-phonon energy of the ^{44}Ca core).

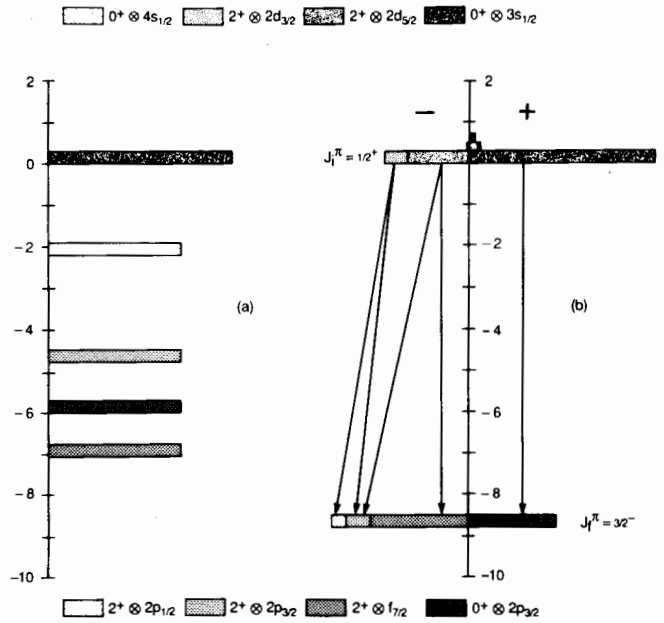

FIG. 4. Illustration of the components in a radiative transition. Part (a) is for the idealized "rigid" spherical nucleus. The bar for the initial state indicates the wave function constructed from the R-matrix states [i.e., it is proportional to $\sum_q \gamma_{q(n)} U_q/(E_q-E)$, where U_q is the wave function for the configuration $0^+ \otimes 3s_{1/2}$; higher $s_{1/2}$ contribution is neglected]. The bars for the final states indicate wave functions for configurations connoted by the same shading as in Fig. 2. An E1 transition is only possible from the initial state to the $0^+ \otimes 2p_{3/2}$ state. Part (b) illustrates the effect of vibrational coupling. There are three sets of bars for the initial state representing the contributions from the three lowest R-matrix states of Fig. 3(b). Only the lowest final state of Fig. 2(b) is shown here. The bars in (b) represent admixture amplitudes rather than intensities; hence signs are indicated. Components of the E1 transition are now possible to different configurations of the final states as shown. Only the components on the right-hand side would be calculated by the unmodified optical model theory. The other components interfere constructively or destructively, depending on their phases.

chosen channel radius of 9.03 fm (at which we cut-off the rapidly attenuating tail of the Woods-Saxon potential) the most important R-matrix states are the $0^+ \otimes 3s_{1/2}$ and $0^+ \otimes 4s_{1/2}$ states shown in Fig. 3(a). The $2^+ \otimes 2d_{5/2}$ and $2^+ \otimes 2d_{3/2}$, which do not affect the s-wave scattering in this idealization, are also shown. The modified form of this portion of the R-matrix state spectrum after introducing the quadrupole coupling is shown in Fig. 3(b). It is apparent that the reduced width of the lowest state, which most strongly affects the scattering at zero neutron energy, is lowered by about 12%, but the energy is lowered by an even more significant factor, so the potential scattering length is greatly changed. The radiation strength from the $0^+ \otimes 3s_{1/2}$ admixture of this and the other R-matrix states (which now carry reduced neutron width amplitudes for s-wave scattering) to the $0^+ \otimes 2p_{3/2}$ component of the lowest final state of Fig. 2(b) is found, as expected, to be rather close to the value computed for the new potential scattering length using the [S] optical-model method as if there were no quadrupole coupling. However, when the radiative transition components from the $2^+ \otimes 2d_{5/2}$ to the $2^+ \otimes 1f_{7/2}$ and $2^+ \otimes 2p_{3/2}$ components of the final state and from the $2^+ \otimes 2d_{3/2}$ to the $2^+ \otimes 2p_{3/2}$ and $2^+ \otimes 2p_{1/2}$ components are all included (see Fig. 4), the capture cross section is reduced to about one-quarter of the optical-model value. The reduction for the next lowest final state is to 40%, while for the two higher states the capture cross section in enchanced by a factor of about 2. When other residual forces are introduced into the Hamiltonian, a sequence of denser and more complex final states will be formed, into which the complex states of Fig. 2(b) will be spread, but in a somewhat local way. It is expected that in this more realistic spectrum the lowest states, for which the detection of electric-dipole gamma rays is enchanced by the E_γ^3 factor and instrumental resolution, will be dominated by the properties of the two lowest states of Fig. 2(b). Hence we can expect a rather systematic reduction (by a factor of about 2) in the capture cross sections for the stronger transitions to the major group of low-lying state from the values computed in the optical-model direct-capture theory.

For ^{26}Mg this model does not lead to significant changes in the potential-capture cross-section. The reason is that the potential scattering length is much less affected by the $3s_{1/2}$ single-particle resonance, and the mixing of the $0^+ \otimes 3s_{1/2}$ configuration with the $2^+ \otimes 2d_{5/2}$ and $2^+ \otimes 2d_{3/2}$ configurations is much weaker, partly owing to the greater separation of the s and d states and partly to the greater vibrational energy (1.81 MeV).

We note in Table 2, however, that there is strong evidence for a weakly bound local level appreciably affecting the thermal capture cross-section. We consider therefore how the properties of local levels may be affected by the collective coupling. We assume first of all that the local levels can be constructed by diagonalizing the nuclear Hamiltonian with all residual forces except the quadrupole vibrational coupling. If two close, just-bound, levels result from this, one with some $0^+ \otimes 3s_{1/2}$ content and the other with $2^+ \otimes 2d_{5/2}$ and $2^+ \otimes 2d_{3/2}$ content, the introduction of the quadrupole coupling could mix these almost equally and push them apart to a degree depending on the magnitude of the quadrupole interaction. If the upper level is thereby pushed much closer to the binding energy and the lower becomes rather more strongly bound there will be a net admixture of the $2^+ \otimes$ d configurations into the initial-state wave function for low-energy neutron interaction. The capture to a quadrupole-coupled final state will be modified as illustrated schematically in Fig. 4 for potential capture, giving rise to rather systematic changes in the capture cross-sections.

This research was sponsored by the U. S. Department of Energy under contract DE-AC05-840R21400 with Martin Marietta Energy Systems, Inc., and by the Underlying Research Program of the U. K. Atomic Energy Authority. Two of us (S.K. and J.E.L.) are grateful to the Oak Ridge National Laboratory for providing kind hospitality.

REFERENCES

1. S. Raman, R.F. Carlton, J.C. Wells, E.T. Jurney, and J.E. Lynn: Phys. Rev. C 32, 18 (1985)
2. S. Raman and J.E. Lynn: Proceedings Fourth International Symposium on Neutron-Induced Reactions, Smolenice, Czechoslovakia, 1985, edited by J. Kristiak and E. Beták (Veda, Bratislava, 1986) p. 253
3. S. Raman and J.E. Lynn: Phys. Rev. Lett. 56, 398 (1986)
4. J.E. Lynn, S. Kahane, and S. Raman: Phys. Rev. C 35, 26 (1987)
5. S. Kahane, J.E. Lynn, and S. Raman: Phys. Rev. C 36, 533 (1987)
6. S. Raman, S. Kahane, and J. E. Lynn: Proceedings Sixth International Symposium on Capture Gamma-Ray Spectroscopy, Leuven, Belgium, 1987, edited by P. Van Assche and K. Abrahams (Inst. Phys. Conf. Ser. No. 88, Bristol, United Kingdom, 1988) J. Phys. G: Nucl. Phys. 14 Suppl. p. S223
7. A.M. Lane and J. E. Lynn: Nucl. Phys. 17, 563 (1960); Nucl. Phys. 17, 586 (1960
8. P.A. Moldauer, Nucl. Phys. 47, 65 (1963)
9. S. Raman, S. Kahane, R.M. Moon, J. Fernandez-Baca, J.L. Zarestsky, J. Richardson, and J.E. Lynn: to be published
10. S.F. Mughabghab, M. Divadeenam, and N.E. Holden, Neuton Cross Sections, Vol. 1, Part A (Academic, New York, 1981)
11. P.A. Moldauer, Nucl. Phys. 47, 65 (1963)
12. A.G.W. Cameron, Can. J. Phys. 37, 322 (1959).